Mechanisms of C−Si and C−H Bond Formation on the Reactions of Alkenylruthenium(II) Complexes with Hydrosilanes

Yooichiroh Maruyama, Kunihiro Yamamura, Takashi Sagawa, Hiroyuki Katayama, and Fumiyuki Ozawa*

Department of Applied Chemistry, Faculty of Engineering, Osaka City University, Sumiyoshi-ku, Osaka 558-8585, Japan

Received November 15, 1999

Reactions of the four alkenylruthenium(II) complexes Ru[C(R^1)═CH(R^2)]Cl(CO)(PPh_3)$_2$ (R^1 = H, R^2 = Ph (**1b**); R^1 = H, R^2 = *t*-Bu (**1c**); R^1 = Ph, R^2 = Ph (**1d**); R^1 = CH═CH($SiMe_3$), R^2 = $SiMe_2Ph$ (**1e**)) with $HSiMe_2Ph$, which constitute the product-forming step of ruthenium-catalyzed hydrosilylation of alkynes, have been examined. Two reaction courses are operative: one provides the C−Si coupling product $PhMe_2SiC(R^1)$═CH(R^2) and RuHCl(CO)-(PPh_3)$_3$ (path A), and the other forms the C−H coupling product HC(R^1)═CH(R^2) and Ru($SiMe_2Ph$)Cl(CO)(PPh_3)$_2$ (path B). The ratio of the two courses significantly varies with substituents on the alkenyl ligands, particularly with the α-substituent (R^1). Thus, **1b** and **1c**, without an α-substituent, react mainly by path A. In contrast, **1d** and **1e**, bearing an α-substituent, exclusively undergo path B. Kinetic studies using **1b** and its para-substituted styryl ligand derivatives have revealed that path A proceeds by direct interaction of the five-coordinated complexes with hydrosilane, without dissociation of the PPh_3 ligand. On the other hand, path B involves dissociation of PPh_3 prior to the reaction of **1d** or **1e** with hydrosilane. Mechanisms of the C−Si and C−H bond formation are discussed with kinetic data in detail.

Introduction

Catalytic hydrosilylation of alkenes and alkynes is a versatile synthetic means of obtaining organosilicon compounds.[1] This catalysis is generally thought to proceed by either the Chalk−Harrod mechanism[2] or the modified Chalk−Harrod mechanism.[3] Although there are several variations,[4,5] the essential features of the catalytic cycles can be summarized as depicted in Scheme 1.[6] The former mechanism (cycle CH) invokes insertion of alkene (or alkyne) into a metal−hydrogen bond (process i), whereas the latter (cycle mCH) invokes insertion into a metal−silicon bond (process iii). Hydrosilylation products are formed by subsequent C−Si and C−H bond formation reactions (processes ii and iv,

Scheme 1

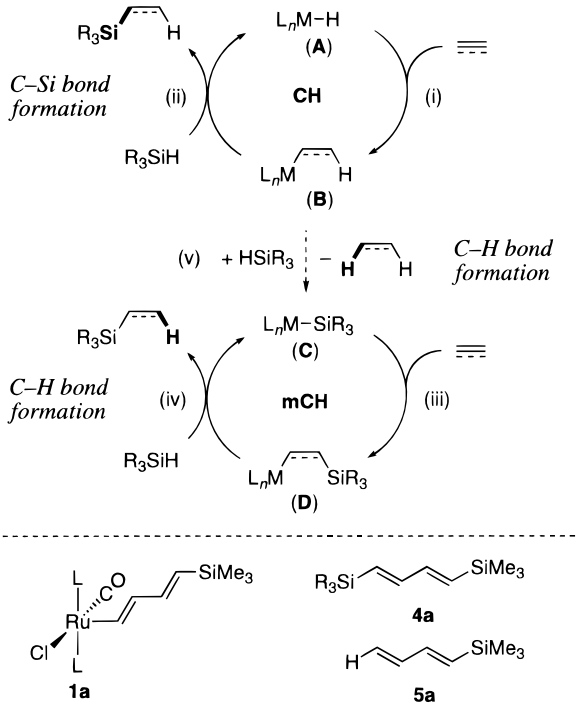

(1) (a) Hiyama, T.; Kusumoto, T. In *Comprehensive Organic Synthesis;* Trost, B. M., Fleming, I., Eds.; Pergamon Press: Oxford, U.K., 1991; Vol. 8, p 763. (b) Ojima, I. In *The Chemistry of Organic Silicon Compounds;* Patai, S., Rappoport, Z., Eds.; Wiley: Chichester, U.K., 1989; p 1479.

(2) (a) Chalk, A. J.; Harrod, J. F. *J. Am. Chem. Soc.* **1965**, *87*, 16. (b) Harrod, J. F.; Chalk, A. J. *J. Am. Chem. Soc.* **1965**, *87*, 1133.

(3) (a) Seitz, F.; Wrighton, M. S. *Angew. Chem., Int. Ed. Engl.* **1988**, *27*, 289. (b) Randolph, C. L.; Wrighton, M. S. *J. Am. Chem. Soc.* **1986**, *108*, 3366. (c) Fernández, M. J.; Esteruelas, M. A.; Jiménez, M. S.; Oro, L. A. *Organometallics* **1986**, *5*, 1519. (d) Ojima, I.; Fuchikami, T.; Yatabe, M. *J. Organomet. Chem.* **1984**, *260*, 335. (e) Onopchenko, A.; Sabourin, E. T.; Beach, D. L. *J. Org. Chem.* **1983**, *48*, 5101. (f) Schroeder, M. A.; Wrighton, M. S. *J. Organomet. Chem.* **1977**, *128*, 345.

(4) (a) Stein, J.; Lewis, L. N.; Gao, Y.; Scott, R. A. *J. Am. Chem. Soc.* **1999**, *121*, 3693. (b) LaPointe, A. M.; Rix, F. C.; Brookhart, M. *J. Am. Chem. Soc.* **1997**, *119*, 906. (c) Esteruelas, M. A.; Olivan, M.; Oro, L. A. *Organometallics* **1996**, *15*, 814. (d) Maddock, S. M.; Rickard, C. E. F.; Roper, W. R.; Wright, L. J. *Organometallics* **1996**, *15*, 1793. (e) Hofmann, P.; Meier, C.; Hiller, W.; Heckel, M.; Riede, J.; Schmidt, M. U. *J. Organomet. Chem.* **1995**, *490*, 51. (f) Hostetler, M. J.; Butts, M. D.; Bergman, R. *Organometallics* **1993**, *12*, 65. (g) Esteruelas, M. A.; Herrero, J.; Oro, L. A. *Organometallics* **1993**, *12*, 2377. (h) Bergens, S. H.; Noheda, P.; Whelan, J.; Bosnich, B. *J. Am. Chem. Soc.* **1992**, *114*, 2128. (i) Duckett, S. B.; Pertsz, R. N. *Organometallics* **1992**, *11*, 90. (j) Tanke, R. S.; Crabtree, R. H. *Organometallics* **1991**, *10*, 415. (k) Lewis, L. N. *J. Am. Chem. Soc.* **1990**, *112*, 5998. (l) Hostetler, M. J.; Bergman, R. *J. Am. Chem. Soc.* **1990**, *112*, 8621.

10.1021/om9909035 CCC: $19.00
Publication on Web 03/03/2000

respectively), typically between alkyl (or alkenyl) intermediates (**B** and **D**) and hydrosilanes. These mechanisms have accounted for a number of observations associated with catalytic hydrosilylation. Furthermore, their experimental supports based on the studies of presumed intermediates have been presented in recent years.[4−6] However, the reason for alteration of the catalytic mechanism depending upon catalysts and substrates has not been well-understood, though such information is crucial for designing highly selective catalyses.[7]

We have recently found that the selection of one of the two catalytic cycles in ruthenium-catalyzed hydrosilylation of 1-(trimethylsilyl)-1-buten-3-yne takes place at a product-forming step, which is composed of the reaction of butadienylruthenium intermediate **1a** in Scheme 1 with hydrosilane.[8] Complex **1a** corresponds to intermediate **B** in cycle CH. When the C−Si bond formation affording **4a** (process ii) proceeds, a ruthenium hydride simultaneously formed in the catalytic system starts the Chalk−Harrod cycle. On the other hand, when the C−H bond formation giving **5a** takes place according to process v, a silylruthenium species generated in the system undergoes insertion of 1-(trimethylsilyl)-1-buten-3-yne to start the modified Chalk−Harrod cycle. Therefore, we have been interested in the mechanisms of the C−Si and C−H bond formation reactions.

There are two possible mechanisms for the reaction of organotransition-metal complexes with hydrosilanes. One is a sequence of oxidative addition and reductive elimination, and the other is σ-bond metathesis involving a four-center transition state. The former process is commonly assumed for late-transition-metal-catalyzed reactions.[2−4,9] On the other hand, the latter has been documented for early-transition-metal complexes with a d^0 metal center.[5a,b,10] Recently, the possibility of σ-bond metathesis has been suggested also for late-transition-metal systems mainly by theoretical studies,[11] while its experimental evidence is still limited.[12,13]

In this paper we wish to report our mechanistic studies on the reactions of alkenylruthenium(II) complexes with hydrosilanes.[14] Since **1a** in Scheme 1 is too unstable to be isolated, further study on the mechanisms of C−Si and C−H bond formation was infeasible.

Scheme 2

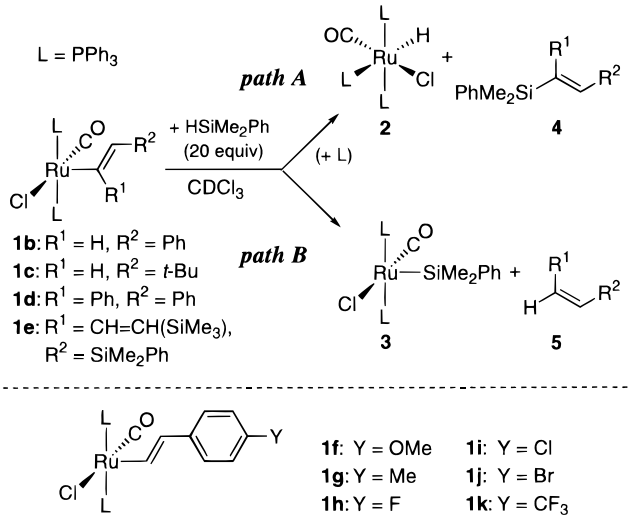

Therefore, we employed in this study four alkenylruthenium complexes which can be isolated (**1b**−**e** in Scheme 2). Kinetic studies have revealed that clearly different mechanisms are operative for the C−Si and C−H bond formation, respectively. Thus, the C−Si bond formation proceeds by direct interaction of the five-coordinated complex with hydrosilane without dissociation of PPh_3 ligand, while the C−H bond formation involves prior dissociation of PPh_3.

Results and Discussion

Reactions of Alkenylruthenium Complexes with $HSiMe_2Ph$. The reactions of **1b**−**e** with $HSiMe_2Ph$ in $CDCl_3$ (Scheme 2) were examined by NMR spectroscopy and GC−mass spectrometry. Table 1 summarizes the results. All of the reactions proceeded at 30 °C by two reaction courses (path A and path B), giving the C−Si coupling product **4** and the C−H coupling product **5**, respectively. The selectivities listed in the table are based on relative ratios of **4** to **5** determined by ^1H NMR spectroscopy. The formation of **4** by path A was accompanied by generation of a hydridoruthenium complex, which was identified as $RuHCl(CO)(PPh_3)_3$ (**2**) when the reaction was carried out in the presence of added PPh_3. However, since the hydride complex is in need of three PPh_3 ligands to be stabilized while the starting **1** possesses only two PPh_3 ligands, the hydride complex could not be detected in the absence of added

(5) (a) Fu, P. E.; Brard, L.; Li, Y.; Marks, T. J. *J. Am. Chem. Soc.* **1995**, *117*, 7157. (b) Kesti, M. R.; Waymouth, R. M. *Organometallics* **1992**, *11*, 1095. (c) Takahashi, T.; Hasegawa, M.; Suzuki, N.; Saburi, M.; Rousset, C. J.; Fanwick, P. E.; Negishi, E. *J. Am. Chem. Soc.* **1991**, *113*, 8564.

(6) (a) Brunstein, P.; Knorr, M. *J. Organomet. Chem.* **1995**, *500*, 21. (b) Tilley, T. D. In *The Chemistry of Organic Silicon Compounds*; Patai, S., Rappoport, Z., Eds.; Wiley: Chichester, U.K., 1989; p 1415. (c) Recatto, C. A. *Aldrichim. Acta* **1995**, *28*, 85.

(7) The relative ease of the Chalk−Harrod and modified Chalk−Harrod mechanisms has been theoretically examined: (a) Sakaki, S.; Mizoe, N.; Sugimoto, M. *Organometallics* **1998**, *17*, 2510. (b) Sakaki, S.; Ogawa, M.; Musashi, Y.; Arai, T. *J. Am. Chem. Soc.* **1994**, *116*, 7258. (c) Sugimoto, M.; Yamasaki, I.; Mizoe, N.; Anzai, M.; Sakaki, S. *Theor. Chem. Acc.* **1999**, *102*, 377−384.

(8) Maruyama, Y.; Yamamura, K.; Nakayama, I. Yoshiuchi, K. Ozawa, F. *J. Am. Chem. Soc.* **1998**, *120*, 1421.

(9) (a) Aizenberg, M.; Milstein, D. *J. Am. Chem. Soc.* **1995**, *117*, 6456. (b) Van der Boom, M. E.; Ott, J.; Milstein, D. *Organometallics* **1998**, *17*, 4263.

(10) (a) Voskoboynikov, A. Z.; Parshina, I. N.; Shestakova, A. K.; Butin, K. P.; Beletskaya, I. P.; Kuz'mina, L. G.; Howard, J. A. K. *Organometallics* **1997**, *16*, 4041. (b) Radu, N. S.; Tilley, T. D. *J. Am. Chem. Soc.* **1995**, *117*, 5863. (c) Woo, H.-G.; Walzer, J. F.; Tilley, T. D. *J. Am. Chem. Soc.* **1992**, *114*, 7047.

(11) (a) Maseras, F.; Duran, M.; Lledós, A.; Bertrán, J. *J. Am. Chem. Soc.* **1992**, *114*, 2922. (b) Musaev, D. G.; Mebel, A. M.; Morokuma, K. *J. Am. Chem. Soc.* **1994**, *116*, 10693. (c) Siegbahn, P. E. M.; Crabtree, R. H. *J. Am. Chem. Soc.* **1996**, *118*, 4442. (d) Su, M.-D.; Chu, S.-Y. *J. Am. Chem. Soc.* **1997**, *119*, 5373. (e) Hutschka, F.; Dedieu, A.; Eichberger, M.; Fornika, R.; Leitner, W. *J. Am. Chem. Soc.* **1997**, *119*, 4432. (f) Milet, A.; Dedieu, A.; Kapteijn, G.; van Koten, G. *Inorg. Chem.* **1997**, *36*, 3223.

(12) (a) Luo, X.-L.; Crabtree, R. H. *J. Am. Chem. Soc.* **1989**, *111*, 2527. (b) Hartwig, J. F.; Bhandari, S.; Rablen, P. R. *J. Am. Chem. Soc.* **1994**, *116*, 1839. (c) Iverson, C. N.; Smith, M. R., III. *J. Am. Chem. Soc.* **1995**, *117*, 4403. (d) Lee, J. C., Jr.; Peris, E.; Rheingold, A. L.; Crabtree, R. H. *J. Am. Chem. Soc.* **1994**, *116*, 11014. (e) Marder, T. B.; Norman, N. C.; Rice, C. R.; Robins, E. G. *Chem. Commun.* **1997**, 53.

(13) For reviews on σ-bond metathesis, see: (a) Arndtsen, B. A.; Bergman, R. G.; Mobley, T. A.; Peterson, T. H. *Acc. Chem. Res.* **1995**, *28*, 154. (b) Crabtree, R. H. *Chem. Rev.* **1995**, *95*, 987.

(14) Portions of this work have been communicated: Maruyama, Y.; Yamamura, K.; Ozawa, F. *Chem. Lett.* **1998**, 905.

Table 1. Reactions of 1b−e with $HSiMe_2Ph$ (20 equiv)[a]

run	complex	PPh_3[b] (equiv/**1**)	selectivity (%)[c] path A	path B
1	**1b**	0	100	0
2	**1b**	1	99	1
3	**1c**	0	67	33
4	**1c**	0.5	78	22
5	**1c**	1	91	9
6	**1c**	2	93	7
7	**1d**	0	0	100
8	**1d**	1	0	100
9	**1e**	0	0	100
10[d]	**1e**	1	0	100

[a] All reactions were run in $CDCl_3$ at 30 °C. [b] The amount of PPh_3 initially added to the system. [c] The selectivity was based on the ratio of **4** to **5**, determined by ^1H NMR spectroscopy. [d] The reaction also gave a small amount (ca. 4%) of $PhMe_2SiC{\equiv}CCH{=}CHSiMe_3$, which is not the reaction product with $HSiMe_2Ph$ but a β-hydrogen elimination product from **1e**.[8]

PPh_3 due to decomposition. On the other hand, when path B was operative, corresponding amounts of silyl complex **3** were formed in the reaction systems irrespective of the presence or absence of added PPh_3. The C−H coupling product formed from **1e** (runs 9 and 10) was a 9:1 mixture of the two structural isomers $PhMe_2SiCH{=}C{=}CHCH_2SiMe_3$ (**5e′**) and $PhMe_2SiCH{=}CHCH{=}CHSiMe_3$ (**5e″**). As already mentioned in the previous paper,[8] the minor product **5e″** is formed directly from **1e**, while the major product **5e′** is produced via a 1,3-shift of the $RuCl(CO)(PPh_3)_2$ moiety along the 2-butadienyl ligand in **1e**.

As seen from Table 1, the ratio of path A to path B significantly varied with substituent(s) on the alkenyl ligands, particularly with α-substituent (R^1). Thus, **1b** and **1c**, without the α-substituent, reacted mainly by path A (runs 1−6). On the other hand **1d** and **1e**, bearing an α-substituent, reacted selectively by path B (runs 7−10). The selectivities for **1b** and **1d** were little affected by addition of PPh_3 to the systems. In contrast, in the reaction of **1c**, the ratio of path A to path B increased as the amount of added PPh_3 increased (runs 3−6). These results indicate a steric control of the reaction course. In the following sections, we first examine the mechanisms of path A and path B by kinetic experiments and then discuss the reason for the change of reaction course depending on the alkenyl ligands.

Kinetic Studies on the Mechanism of Path A. Styryl complex **1b** was treated with an excess amount of $HSiMe_2Ph$ (>8.2 equiv) in $CDCl_3$ in the presence or absence of added PPh_3, and the time course was followed by ^1H NMR spectroscopy. In the presence of added PPh_3, the reaction was first-order in the concentration of **1b** over 90% conversion. On the other hand, since the reaction in the absence of added PPh_3 was accompanied by decomposition of a hydridoruthenium species (vide supra), the reaction rate was estimated at low conversion of **1b** (up to 44%), where the first-order plot exhibited a good linear correlation, including the origin.

Table 2 lists the rate constants measured under various conditions. The reaction rate increased linearly as the concentration of $HSiMe_2Ph$ increased (runs 1−5, $r^2 = 0.998$). The relation observed was in good agreement with the ideal second-order rate expression given in eq 1. On the other hand, the reaction rate was little dependent upon the concentration of free PPh_3 (runs 4 and 6−8).

Table 2. Pseudo-First-Order Rate Constants for the Reaction of 1b with $HSiMe_2Ph$ under Various Conditions[a]

run	$[HSiMe_2Ph]$ (mM)	$[PPh_3]$ (mM)	reacn temp (°C)	$10^3 k_{obsd}$ (s^{-1})
1	82	10	10.0	0.550(5)
2	99	10	10.0	0.66(2)
3	151	10	10.0	1.06(2)
4	200	10	10.0	1.34(1)
5	285	10	10.0	2.02(6)
6	200	0	10.0	1.5(1)
7	200	20	10.0	1.26(3)
8	200	30	10.0	1.18(1)
9	200	10	0.0	0.738(9)
10	200	10	20.0	2.32(4)
11	200	10	30.0	3.86(5)

[a] All reactions were run in $CDCl_3$. Initial concentration: $[\mathbf{1b}]_0 = 10.0$ mM.

Scheme 3

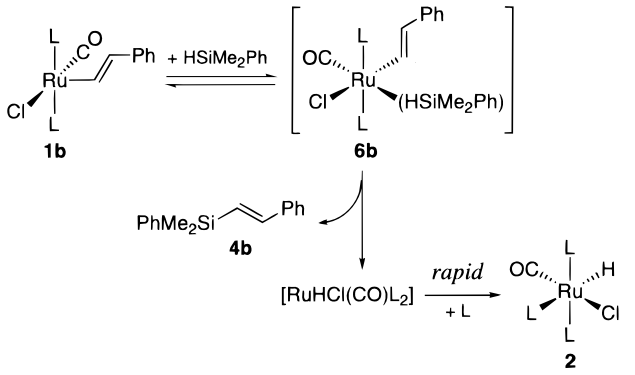

$$-d[\mathbf{1b}]/dt = k_{2nd}[HSiMe_2Ph]^{1.04(2)}[\mathbf{1b}] \qquad (1)$$

$$k_{2nd} = [7.0(1)] \times 10^{-3}\ s^{-1}\ M^{-1} \text{ at } 10\ °C$$

These kinetic data indicate the reaction process depicted in Scheme 3. The first step is the coordination of hydrosilane to styryl complex **1b**.[15] Considering a small influence of added PPh_3, this step is assumed to proceed mainly without dissociation of the PPh_3 ligand. The resulting **6b** affords the C−Si coupling product **4b** and $RuHCl(CO)(PPh_3)_2$. In the presence of added PPh_3, the latter rapidly combines with PPh_3 to give **2**.

There are two possible mechanisms for the formation of **4b** and $RuHCl(CO)(PPh_3)_2$ from **6b** (Scheme 4). One is the σ-bond metathesis involving the four-center transient species **7b** (mechanism I), while the other proceeds by oxidative addition of coordinated hydrosilane, followed by C−Si reductive elimination from the resulting hydrido−silyl−styryl species **8b** (mechanism II). Mechanism I can take place directly from **6b** in least motion. On the other hand, since **6b** is coordinatively saturated, the oxidative addition in mechanism II must involve prior dissociation of one of the PPh_3 ligands. Although this situation does not simply agree with the kinetic data, showing little retardation effect of added

(15) While the coordination mode of hydrosilane is not defined in this paper, the η^2 coordination of hydrosilane seems the most probable one. Such structures have been established for many transition-metal complexes.[16]

Scheme 4

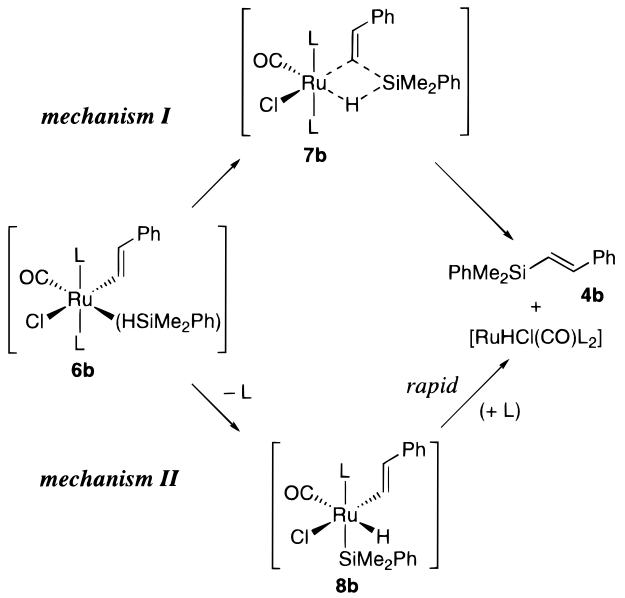

Table 3. Pseudo-First-Order and Second-Order Rate Constants for the Reactions of Ru{CH=CH(C_6H_4Y-*p*)}Cl(CO)(PPh_3)$_2$ (1f−k) with $HSiMe_2Ph$[a]

run	complex (Y)	σ_p^+	σ_p	10^3k_{obsd} (s^{-1})	10^3k_{2nd} (s^{-1} M^{-1})
1	**1f** (OMe)	−0.778	−0.268	5.1(2)	25(1)
2	**1g** (Me)	−0.311	−0.17	1.38(3)	6.89(2)
3	**1h** (F)	−0.073	0.062	1.43(3)	7.17(2)
4	**1b** (H)	0	0	0.738(9)	3.69(4)
5	**1i** (Cl)	0.114	0.227	0.470(5)	2.35(2)
6	**1j** (Br)	0.15	0.232	0.44(1)	2.18(4)
7	**1k** (CF_3)	0.612	0.54	0.170(5)	0.850(3)

[a] All reactions were run in $CDCl_3$ at 0.0 °C in the presence of added PPh_3. Initial concentration: $[\mathbf{1}]_0 = 10.0$ mM, $[HSiMe_2Ph]_0 = 200$ mM, $[PPh_3]_0 = 10.0$ mM. The second-order rate constants (k_{2nd}) were obtained by dividing the pseudo-first-order rate constants (k_{obsd}) by the initial concentration of $HSiMe_2Ph$.

PPh_3, mechanism II may still be possible when the dissociation of PPh_3 from **6b** takes place simultaneously with the oxidative addition and the successive C−Si reductive elimination proceeds rapidly.[17] To distinguish mechanisms I and II, a variety of substituents were introduced into **1b** and $HSiMe_2Ph$, and their effect on the reaction rate was investigated.

Table 3 summarizes the rate constants for **1f**−**k** bearing a variety of substituents at the para position of the styryl ligand (see Scheme 2 for numbering), which were measured under the same reaction conditions as run 9 in Table 2. The more electron-releasing substituent tended to provide the higher reaction rate. Among various Hammett parameters tested, σ_p^+ values of the substituents exhibited the most satisfactory Hammett correlation with the rate constants (Figure 1): $\rho = -1.07(4)$, $r^2 = 0.993$ except for **1h** (Y = F).[18] On the other hand, Hammett correlation between the k_{obsd} and σ_p values was low ($r^2 = 0.878$).[19]

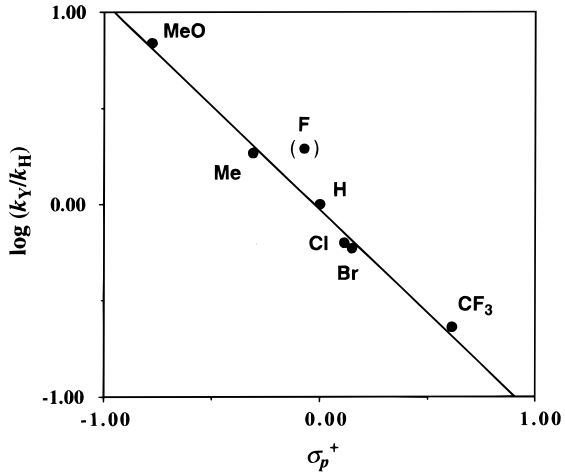

Figure 1. Hammett plot for the data in Table 3.

Table 4. Pseudo-First-Order and Second-Order Rate Constants for the Reactions of 1b with Various Hydrosilanes[a]

run	hydrosilane	σ_p	react temp (°C)	10^3k_{obsd} (s^{-1})	10^3k_{2nd} (s^{-1} M^{-1})
1	$HSiMe_2$–C$_6$H$_4$–OMe	−0.268	0.0	0.97(2)	4.9(1)
2	$HSiMe_2$–C$_6$H$_4$–Me	−0.17	0.0	0.65(1)	3.3(1)
4	$HSiMe_2$–C$_6$H$_5$	0	0.0	0.738(9)	3.69(5)
3	$HSiMe_2$–C$_6$H$_4$–F	0.062	0.0	0.98(2)	4.9(1)
5	$HSiMe_2$–C$_6$H$_4$–Cl	0.227	0.0	1.27(2)	6.35(1)
6	$HSiMe_2$–C$_6$H$_4$–Br	0.232	0.0	1.61(4)	8.05(2)
7	$HSiMe_2$–C$_6$H$_4$–CF_3	0.54	0.0	2.02(5)	1.01(2)
8	$HSiMe_2Ph$	—	30.0	3.86(5)	1.93(2)
9	$HSiMePh_2$	—	30.0	0.231(3)	1.15(2)
10	$HSiPh_3$	—	30.0	very slow[b]	

[a] All reactions were run in $CDCl_3$ in the presence of added PPh_3. Initial concentration: $[\mathbf{1b}]_0 = 10.0$ mM, [hydrosilane]$_0 = 200$ mM, $[PPh_3]_0 = 10.0$ mM. The second-order rate constants (k_{2nd}) were obtained by dividing the pseudo-first-order rate constants (k_{obsd}) by the initial concentration of $HSiMe_2Ph$. [b] The reaction was too slow to perform a kinetic run, which is complete after ca. 55 h at 30 °C.

Reactivities of a series of para-substituted dimethylphenylsilanes were compared for the reactions with **1b**. The results are listed in runs 1−7 of Table 4. The more electron-withdrawing substituent tended to pro-

(16) (a) Crabtree, R. H. *Angew. Chem., Int. Ed. Engl.* **1993**, *32*, 789. (b) Schubert, U. *Adv. Organomet. Chem.* **1990**, *30*, 151. (c) Spaltenstein, E.; Palma, P.; Kreutzer, K. A.; Willoughby, C. A.; Davis, W. M.; Buchwald, S. L. *J. Am. Chem. Soc.* **1994**, *116*, 10308. (d) Luo, X.-L.; Kubas, G. J.; Bryan, J. C.; Burns, C. J.; Unkefer, C. J. *J. Am. Chem. Soc.* **1994**, *116*, 10312. (e) Luo, X.-L.; Kubas, G. J.; Burns, C. J.; Bryan, J. C.; Unkefer, C. J. *J. Am. Chem. Soc.* **1995**, *117*, 1159. (f) Corey, J. Y.; Broddock-Wilking, J. *Chem. Rev.* **1999**, *99*, 175.

(17) The kinetic expression given in eq 1 is also consistent with the mechanism involving the rate-determining formation of **6b**. However, this mechanism is incompatible with the kinetic data for a series of para-substituted $HSiMe_2Ph$ and styryl complexes. Thus, in this situation, the more electron-rich hydrosilane and the more electron-deficient ruthenium center should provide the higher reaction rate if steric conditions are similar. However, the reactivity order observed for a series of para-substituted dimethylphenylsilane derivatives was apparently opposite to this prospect (Figure 2). In addition, although the more electron-withdrawing substituent Y at the para position of the styryl ligand possibly causes the ruthenium center to be more electron deficient and thereby a higher reaction rate, the reactivity order actually observed was just the reverse (Figure 1).

(18) The data including **1h**: $\rho = -1.1(1)$; $r^2 = 0.956$.

(19) The other Hammett parameters tested were σ_p^0 and σ_i. The correlation coefficients (r^2) for least-squares calculations are 0.848 and 0.215, respectively.

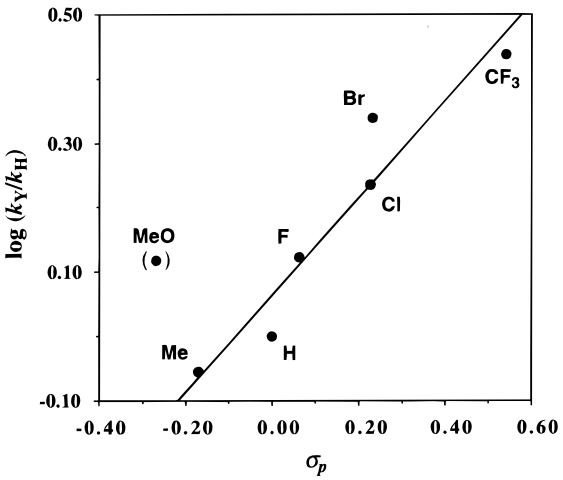

Figure 2. Hammett plot for the data in runs 1−7 in Table 4.

Scheme 5

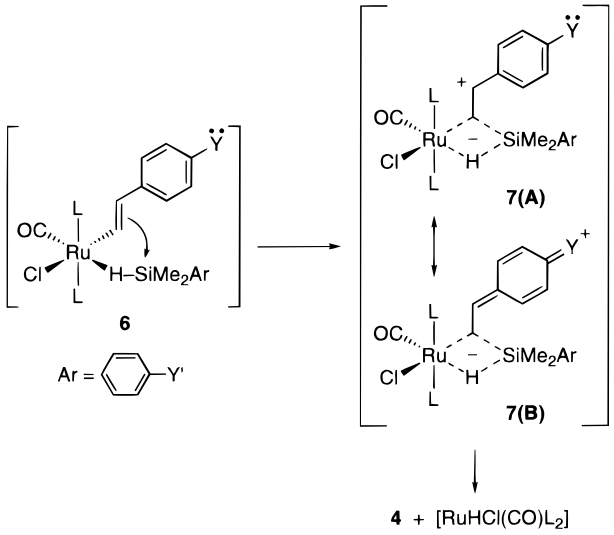

vide the higher reactivity. Except for the data of dimethyl(*p*-methoxyphenyl)silane in run 1, the rate constants exhibited a fair Hammett correlation with the σ_p values of substituents (ρ = 0.76(11); r^2 = 0.917) (Figure 2). On the other hand, reactivities of three silanes in runs 8−10 decreased in the order $HSiMe_2Ph$ > $HSiMePh_2$ ≫ $HSiPh_3$, probably reflecting the increasing bulkiness.

These kinetic observations can be reasonably interpreted by mechanism I in Scheme 4. Thus, the Hammett correlations given in Figures 1 and 2 indicate nucleophilic attack of the styryl ligand on the coordinated hydrosilane to take place. As depicted by the limiting structure **7(A)** in Scheme 5, this process will produce a carbocation at the para position of the substituent, which is stabilized by the resonance structure **7(B)**. The good Hammett correlation for σ_p^+ values in Figure 1 is fully consistent with this mechanism; the σ_p^+ values are known to reflect stabilization of an α-cationic center generated at the para position of the substituent in the transition state.[20]

(20) (a) Inamoto, N. *Hammett Soku (The Hammett Rule)*; Maruzen: Tokyo, 1983. (b) Brown, H. C.; Okamoto, Y. *J. Am. Chem. Soc.* **1958**, *80*, 4979.

Table 5. Activation Parameters and Deuterium Kinetic Isotope Effect for the Reactions of Styryl Complexes 1b,f,k with $HSiMe_2Ph$[a,b]

1f (Y = OMe)	$\Delta H^‡$ = 12.0(2) kcal mol^{-1}	$\Delta S^‡$ = −21.9(8) eu
	k_H/k_D = 0.93(7)	
1b (Y = H)	$\Delta H^‡$ = 8.51(2) kcal mol^{-1}	$\Delta S^‡$ = −38.3(1) eu
	k_H/k_D = 1.00(3)	
1k (Y = CF_3)	$\Delta H^‡$ = 6.67(5) kcal mol^{-1}	$\Delta S^‡$ = −48.0(2) eu
	k_H/k_D = 1.3(1)	

[a] The activation parameters were estimated from Eyring plots of the second-order rate constants measured in $CDCl_3$ in the presence of added PPh_3. Initial concentration: $[\mathbf{1}]_0$ = 10.0 mM, $[HSiMe_2Ph]_0$ = 200 mM, $[PPh_3]_0$ = 10.0 mM. Temperature range: −35.0−0.0 °C for **1f** (r^2 = 0.999 for 5 data points), 0.0−30.0 °C for **1b** (r^2 = 1.00 for 4 data points), 0.0−35.0 °C for **1k** (r^2 = 1.00 for 4 data points). [b] The k_D values were measured using $DSiMe_2Ph$ (200 mM) in place of $HSiMe_2Ph$ at 0.0 °C in $CDCl_3$ in the presence of added PPh_3 (10.0 mM).

On the other hand, mechanism II in Scheme 4 was found to be less compatible with the experimental results. Since the oxidative addition of hydrosilane proceeds via a back-donating interaction between a filled d orbital on the ruthenium and the H−Si σ* orbital,[16a] the more electron-rich ruthenium center and the more electron-deficient hydrosilane will provide the higher reaction rate if steric conditions are similar. This prospect is consistent with the Hammett correlation observed for a series of para-substituted $HSiMe_2Ph$ (Figure 2). However, the electron density of the ruthenium center was found to be insensitive to the para substituents Y on the styryl ligands. Thus, the styryl complex derivatives listed in Table 3 exhibited the same $^{31}P\{^1H\}$ NMR chemical shifts (δ 31.4(2)) and almost the same ν(CO) frequencies (1924(2) cm^{-1}, except for **1h** (1912 cm^{-1})). This fact clearly indicates that the Y groups are situated too far from the ruthenium center to affect the electron density. Consequently, it is hard to rationalize the distinct Hammett correlation observed from Figure 1 by mechanism II.

Table 5 lists the kinetic parameters for **1b**, **1f**, and **1k**. All of the reactions exhibited a large negative entropy, in agreement with the associative mechanism in Schemes 3 and 5. The magnitude increased significantly as the reactivity of the complex decreased (**1f** > **1b** > **1k**). Deuterium kinetic isotope effects observed with $DSiMe_2Ph$ were negligible for **1b** and **1f**, while a small isotope effect beyond the experimental error was noted for **1k** with the least reactivity.

These kinetic parameters can be rationalized by considering variations in the transition-state structures between **6** and **7** in Scheme 5. As judged from the k_H/k_D values, the exact transition state seems very close to **6** for all complexes. However, the clear Hammett correlation in Figure 1 and a distinct tendency for the kinetic parameters in Table 5 strongly suggest the occurrence of such variation dependent upon the para substituents Y. Thus, when the styryl ligand is highly nucleophilic due to the presence of an electron-releasing substituent, the nucleophilic attack on the coordinated hydrosilane may take place with the least activation barrier after the formation of **6**. The relatively small activation entropy observed for **1f** (Y = OMe) is consistent with this situation. In this case, elongation of the H−Si bond in the transition state should be negligible, and therefore no kinetic isotope effect can be observed. In contrast, when an electron-withdrawing substituent

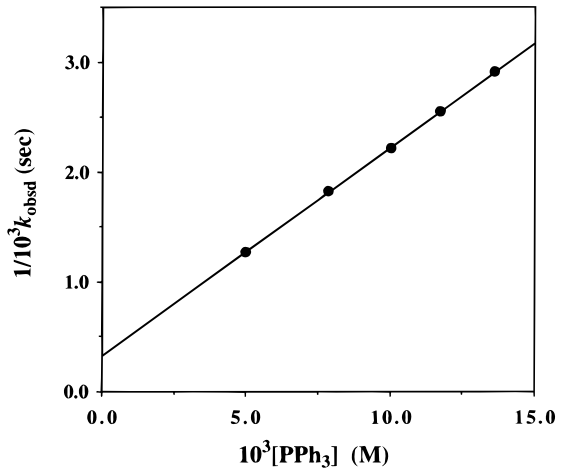

Figure 3. Effect of added PPh_3 on the reaction rate of **1d** with $HSiMe_2Ph$ in $CDCl_3$ at 45 °C. Initial concentration: $[\mathbf{1d}]_0 = 10.0$ mM, $[HSiMe_2Ph]_0 = 200$ mM.

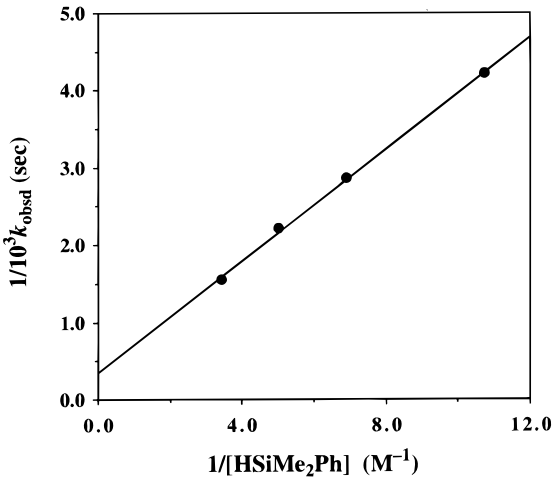

Figure 4. Effect of $HSiMe_2Ph$ concentration on the reaction rate of **1d** with $HSiMe_2Ph$ in $CDCl_3$ at 45 °C in the presence of added PPh_3. Initial concentration: $[\mathbf{1d}]_0 = 10.0$ mM, $[PPh_3]_0 = 10.0$ mM.

such as CF_3 in **1k** reduces the nucleophilicity of the styryl ligand, the transition state may somewhat shift its position from **6** toward **7**. In this situation, the more restricted structure with an elongated H−Si bond leads to the larger negative entropy and the observable isotope effect.

Kinetic Studies on the Mechanism of Path B. We next carried out kinetic experiments on path B using **1d** and **1e**.[21] Distinct from **1b**, both complexes underwent dissociation of PPh_3 prior to the reaction with $HSiMe_2Ph$.

(a) With 1d. The reaction of **1d** with $HSiMe_2Ph$ in $CDCl_3$ obeyed good pseudo-first-order kinetics with respect to the concentration of **1d** over 90% conversion when an excess amount of the hydrosilane (>9.3 equiv) was present. The reaction progress was effectively suppressed by addition of free PPh_3 to the system; a good linear correlation between $1/k_{obsd}$ values and the concentration of added PPh_3 ($r^2 = 1.000$) was observed (Figure 3). Furthermore, $1/k_{obsd}$ values varied in proportion to $1/[HSiMe_2Ph]$ values ($r^2 = 0.999$) (Figure 4).[22a]

These kinetic observations indicate the mechanism given in Scheme 6. The first step is dissociation of one of the PPh_3 ligands from **1d**. This assumption is supported by the strong retardation effect of added PPh_3. It is also assumed that the dissociation of PPh_3 is accompanied by coordination of the α-phenyl group of alkenyl ligand to the ruthenium center, because **1d** is a 16e complex and dissociation of PPh_3 without an incoming ligand leads to a high-energy process involving a 14e species. Although the solvent-induced dissociation is possible, no significant variation in the reaction rates was observed with three kinds of solvents ($CDCl_3$, C_6D_6, THF-d_8).[22b] The resulting **8d** reacts with $HSiMe_2Ph$ to give stilbene **5d** and a coordinatively unsaturated silyl complex; the latter subsequently combines with free PPh_3 in the system to afford silyl complex **3**.

Steady-state approximation for the concentration of **8d** leads to the equation

$$d[\mathbf{8d}]/dt = k_1[\mathbf{1d}] - k_{-1}[PPh_3][\mathbf{8d}] - k_2[HSiMe_2Ph][\mathbf{8d}] = 0 \quad (2)$$

Thus

$$[\mathbf{8d}] = \frac{k_1[\mathbf{1d}]}{k_{-1}[PPh_3] + k_2[HSiMe_2Ph]} \quad (3)$$

Consequently, the rate of the consumption of **1d** and the k_{obsd} value are expressed by eqs 4 and 5, respectively, which are fully consistent with the relations observed from Figures 3 and 4.

$$-\frac{d[\mathbf{1d}]}{dt} = k_2[HSiMe_2Ph][\mathbf{8d}] = \frac{k_1k_2[HSiMe_2Ph]}{k_{-1}[PPh_3] + k_2[HSiMe_2Ph]}[\mathbf{1d}] \quad (4)$$

$$\frac{1}{k_{obsd}} = \frac{k_{-1}[PPh_3]}{k_1k_2[HSiMe_2Ph]} + \frac{1}{k_1} \quad (5)$$

Thus, the k_{-1}/k_1k_2 values, which are estimated from the slopes of the plots in Figures 3 and 4, are in good agreement with each other: $[3.80(4)] \times 10^4$ and $[3.61(9)] \times 10^4$ s. In addition, reciprocals of the intercepts in these figures, which correspond to the rate constant k_1 for the dissociation of PPh_3 ligand from **1d**, are in good accord with each other: $[3.0(2)] \times 10^{-3}$ and $[2.8(5)] \times 10^{-3}$ s^{-1}.

(b) With 1e. It was found that the dissociation of PPh_3 from **1d** is a slow process.[22c] Consequently, further information on the mechanism of path B, particularly on the interaction between the alkenylruthenium center and hydrosilane, could not be gained with **1d**. In

(21) A listing of the rate constants for **1d** and **1e** is available in the Supporting Information.

(22) (a) Kinetic parameters for **1d** estimated from pseudo-first-order rate constants in $CDCl_3$ in the presence of 200 mM of $HSiMe_2Ph$ are as follows: $\Delta H^{\ddagger} = 14.7(6)$ kcal mol^{-1}, $\Delta S^{\ddagger} = -25(2)$ eu, $k_H/k_D = 1.07(3)$ at 30 °C. (b) Pseudo-first-order rate constants measured in three kinds of solvents in the presence of 200 mM of $HSiMe_2Ph$ and 10.0 mM of added PPh_3 at 45 °C are as follows: $[CDCl_3]$, $[4.51(8)] \times 10^{-4}$; $[C_6D_6]$, $[4.16(4)] \times 10^{-4}$; [THF-d_8], $[5.48(7)] \times 10^{-4}$ s^{-1}. (c) The dissociation of PPh_3 should be the slowest process in Scheme 6, because the steady-state approximation for **8d** requires the relation k_{-1}, $k_2 \gg k_1$. However, since $k_{-1} > k_2$ ($k_{-1}/k_2 = [1.0(2)] \times 10^2$), the rate-determining step can be assigned to the process for k_2.[28g]

Scheme 6

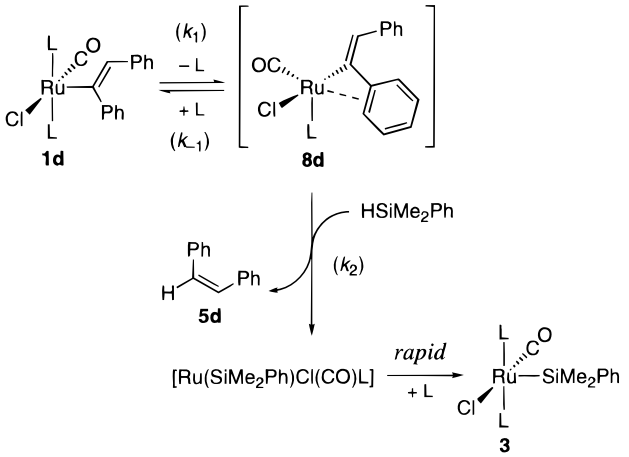

Scheme 7

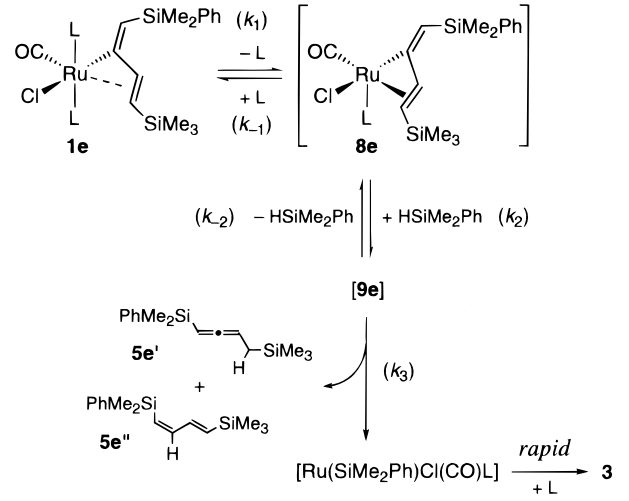

contrast, ^{31}P and ^{1}H NMR signals of the 2-butadienyl complex **1e** in $CDCl_3$ were significantly broadened even at −20 °C, indicating the occurrence of fluxional behavior involving a rapid dissociation of PPh_3. The high reactivity is attributable to an apparently six-coordinate structure of **1e**, in which the $C^3{=}C^4$ bond of the 2-butadienyl ligand is weakly bonded to ruthenium by π-coordination[23] and facilitates the phosphine dissociation (see Scheme 7).

The time course of the reaction of **1e** with $HSiMe_2Ph$ in $CDCl_3$ was followed by ^{1}H NMR spectroscopy. A good first-order dependence on the concentration of **1e** was observed in the presence of an excess amount of $HSiMe_2Ph$ (>9.5 equiv/**1e**). The reaction was much faster than that of **1d**,[24] probably reflecting much easier dissociation of PPh_3 from **1e** than **1d**. The participation of phosphine dissociation in the reaction process was further suggested by the following kinetic data. Thus, the reaction progress was strongly retarded by addition of free PPh_3, and reciprocals of the rate constants ($1/k_{obsd}$) were linearly dependent upon the concentration of added PPh_3 ($r^2 = 0.995$) (Figure 5). A good linear correlation was also observed

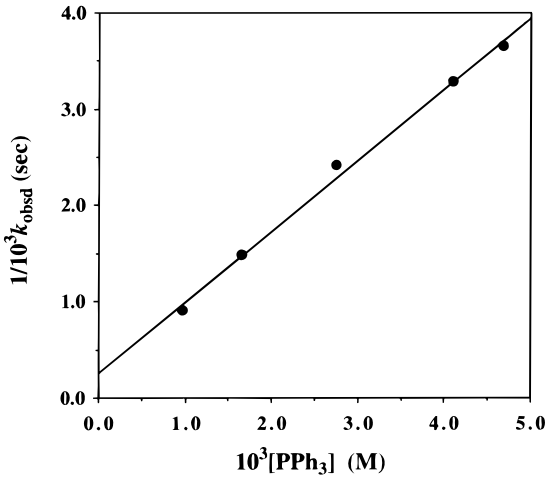

Figure 5. Effect of added PPh_3 on the reaction rate of **1e** with $HSiMe_2Ph$ in $CDCl_3$ at 20 °C. Initial concentration: $[\mathbf{1e}]_0 = 10$ mM, $[HSiMe_2Ph]_0 = 195$ mM.

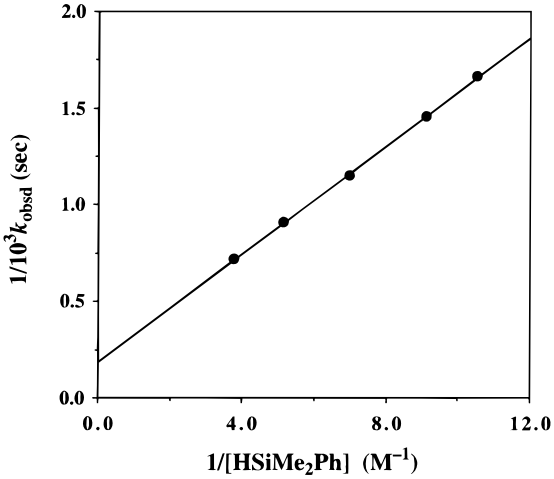

Figure 6. Effect of $HSiMe_2Ph$ concentration on the reaction rate of **1e** with $HSiMe_2Ph$ in $CDCl_3$ at 20 °C in the presence of added PPh_3. Initial concentration: $[\mathbf{1e}]_0 = 10$ mM, $[PPh_3]_0 = 0.968$ mM.

between $1/k_{obsd}$ and $1/[HSiMe_2Ph]$ values ($r^2 = 1.000$) (Figure 6).

Scheme 7 represents our proposed mechanism. As already pointed out, **1e** is in rapid equilibrium with the coordinatively unsaturated species **8e**, which reacts with $HSiMe_2Ph$ to give the C−H coupling products **5e′** and **5e″** and silyl complex **3**. In this scheme, the presence of intermediate **9e** is postulated. This assumption is essential to rationalize the typical saturation kinetic behavior observed for the concentration of $HSiMe_2Ph$ (Figure 6).

When the interconversion between **1e** and **9e** via **8e** is a rapid process, the concentration of **9e** at time t is given by eq 6, where $K_1 = k_1/k_{-1} = [\mathbf{8e}][PPh_3]/[\mathbf{1e}]$, $K_2 = k_2/k_{-2} = [\mathbf{9e}]/[\mathbf{8e}][HSiMe_2Ph]$, and $[Ru(butadienyl)]_{total}$ is the sum of the concentrations of 2-butadienyl ruthenium species at time t (i.e. $[\mathbf{1e}] + [\mathbf{8e}] + [\mathbf{9e}]$).

$$[\mathbf{9e}] = \frac{K_1K_2[HSiMe_2Ph]}{[PPh_3] + K_1 + K_1K_2[HSiMe_2Ph]}[Ru(butadienyl)]_{total} \quad (6)$$

Accordingly, the reaction rate and the k_{obsd} value are

(23) Wakatsuki, Y.; Yamazaki, H.; Maruyama, Y.; Shimizu, I. *J. Organomet. Chem.* **1992**, *430*, C60.

(24) Rate constants observed in $CDCl_3$ at 5.0 °C in the presence of 200 mM of $HSiMe_2Ph$ are as follows: [**1e**], 1.92×10^{-3} s^{-1}; [**1d**], 4.64×10^{-5} s^{-1}.

Scheme 8

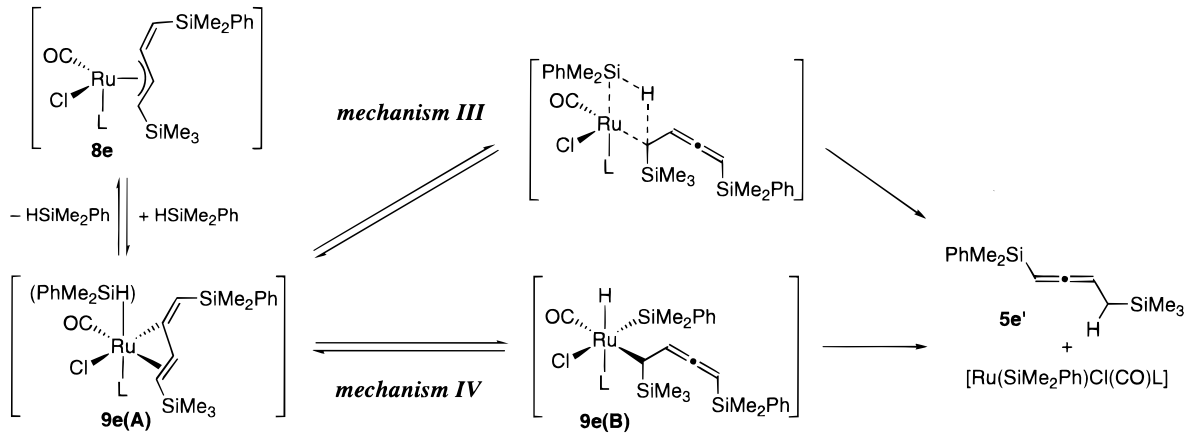

expressed by eqs 7 and 8, respectively.

$$-\frac{d}{dt}[\text{Ru(butadienyl)}]_{\text{total}} = k_3[\mathbf{9e}] = \frac{k_3K_1K_2[\text{HSiMe}_2\text{Ph}]}{[\text{PPh}_3] + K_1 + K_1K_2[\text{HSiMe}_2\text{Ph}]}[\text{Ru(butadienyl)}]_{\text{total}} \quad (7)$$

$$\frac{1}{k_{\text{obsd}}} = \frac{[\text{PPh}_3]}{k_3K_1K_2[\text{HSiMe}_2\text{Ph}]} + \frac{1}{k_3K_2[\text{HSiMe}_2\text{Ph}]} + \frac{1}{k_3} \quad (8)$$

On the basis of the slopes and intercepts of Figures 5 and 6, the following equations are derived from eq 8. From Figure 5 ($[\text{HSiMe}_2\text{Ph}]_{\text{const}} = 195$ mM)

$$\frac{1}{k_3K_1K_2 \times 0.195\ \text{M}} = [7.4(3)] \times 10^5\ \text{s M}^{-1} \quad (9)$$

$$\frac{1}{k_3K_2 \times 0.195\ \text{M}} + \frac{1}{k_3} = [2.7(9)] \times 10^2\ \text{s} \quad (10)$$

From Figure 6 ($[\text{PPh}_3]_{\text{const}} = 0.968$ mM)

$$\frac{0.968 \times 10^{-3}\ \text{M}}{k_3K_1K_2} + \frac{1}{k_3K_2} = 140(1)\ \text{s M} \quad (11)$$

$$\frac{1}{k_3} = [1.91(8)] \times 10^2\ \text{s} \quad (12)$$

Substitution of the $1/k_3$ value of eq 12 for eq 10 leads to $1/k_3K_2 = 15(19)$ s M. On the basis of this value, $1/k_3K_1K_2$ in eq 11 is estimated as $[1.3(2)] \times 10^5$ s, which is in good agreement with the value calculated from eq 9 ($[1.4(1)] \times 10^5$ s). The rate and equilibrium constants most consistent with the data in Figures 5 and 6 are as follows (20 °C): $k_3 = [5.2(2)] \times 10^{-3}\ \text{s}^{-1}$, $K_1K_2 = [1.4(4)] \times 10^{-3}$, $K_1 = 1.1 \times 10^{-4}$ M, $K_2 = 13\ \text{M}^{-1}$.

We described that the kinetic observations for **1e** are reasonably accounted for by the mechanism in Scheme 7, which is composed of a rapid equilibration between **1e** and **9e** and the rate-determining conversion of **9e** into the products. It was further confirmed that an alternative rate expression derived from the steady-state approximation for **9e** is clearly inconsistent with the kinetic data.[25]

The next subject is the identification of the structure of **9e**. Similarly to the reaction of **1b**, two types of mechanisms, the σ-bond metathesis and the sequence of oxidative addition and reductive elimination, are possible for the reaction of **8e** with HSiMe_2Ph. Scheme 8 illustrates those producing the major product **5e′**. The first step, which is common to both of the mechanisms, is the association of HSiMe_2Ph with **8e** to give **9e(A)**.[15] When σ-bond metathesis in mechanism III is operative, **9e(A)** may be assigned to the intermediate **9e** because the subsequent processes must proceed without any stable or metastable intermediates. On the other hand, when mechanism IV takes place, **9e(A)** should be a transient species, while the resultant **9e(B)** is consistent with the intermediate **9e**, because oxidative addition of hydrosilane with late-transition-metal complexes is commonly a low-energy process.[26]

These possibilities could be discriminated from each other on the basis of kinetic parameters measured at a high concentration of HSiMe_2Ph (200 mM) in the absence of added PPh_3. As judging from eq 8, the rate constants observed under such conditions can be approximated to k_3 in Scheme 7. Indeed, k_{obsd} values were nearly constant ($[1.05(6)] \times 10^{-3}\ \text{s}^{-1}$ at 0 °C) independent of the concentration of hydrosilane (182−294 mM). The activation parameters thus obtained are as follows: $\Delta H^{\ddagger} = 20.7(7)$ kcal mol^{-1}, $\Delta S^{\ddagger} = +4(3)$ eu. Since the σ-bond metathesis in mechanism III is expected to involve a significantly large negative entropy arising from a restricted transition state,[13] the observed $\Delta S^{\ddagger}$ value is apparently inconsistent with this mechanism. On the other hand, the activation parameters fall within the range previously reported for the C−H reductive elimination from late-transition-metal complexes.[28] Furthermore, the deuterium isotope effect observed with DSiMe_2Ph ($k_{\text{H}}/k_{\text{D}} = 2.99(9)$) was similar to the values

(25) The steady-state approximation for **9e** leads to the following equation, which does not coincide with the saturation kinetic behavior for the concentration of HSiMe_2Ph in Figure 6: $k_{\text{obsd}} = k_2k_3K_1[\text{HSiMe}_2\text{Ph}]/(k_{-2} + k_3)(K_1 + [\text{PPh}_3])$.

(26) The activation energy ($\Delta G^{\ddagger}$) so far reported for the oxidative addition of hydrosilane toward late-transition-metal complexes falls within the range 8−15 kcal mol^{-1}.[27] However, it is known that, at least for the manganese complexes,[27a,d,f] the activation energy mainly reflects the energy change associated with predissociation of a coordinated solvent such as heptane. Therefore, the actual activation barrier for oxidative addition may be lower than the observed one.

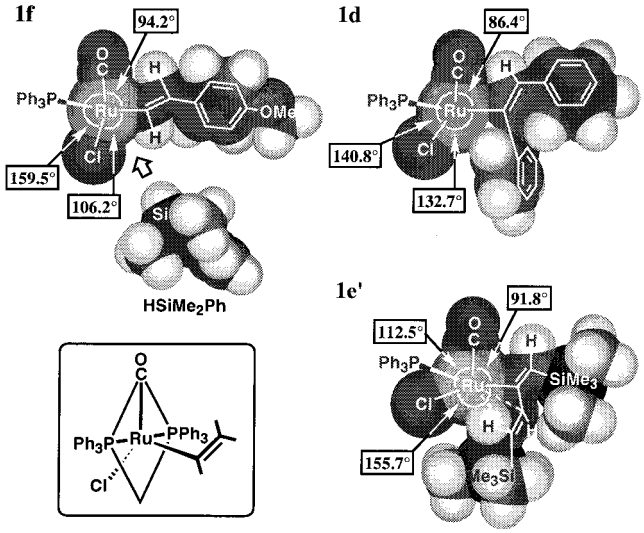

Figure 7. Chem3D views of the X-ray structures of **1f**, **1d**, and the bis(trimethylsilyl) analogue of **1e** (**1e′**). Two PPh_3 ligands are omitted for clarity.

for C−H reductive elimination from *cis*-$PtR(H)(PPh_3)_2$ (R = Me (3.3), CH_2CF_3 (2.2)).[28a,b] Hence, mechanism IV in Scheme 8 has been supported.

Comparison of X-ray Structures. It has been found that clearly distinct processes are operative for path A and path B in Scheme 2, respectively. For path A, the starting alkenylruthenium complex directly reacts with hydrosilane, without dissociation of PPh_3. In contrast, path B involves prior dissociation of PPh_3. Therefore, one may expect a shift of the reaction course from path B to path A by addition of PPh_3 to the system. The change in the selectivity observed for **1c** (runs 3−6 in Table 1) should be the case. In contrast, no trace of C−H coupling products derived from path A were observed for **1d** and **1e** even in the presence of free PPh_3 (runs 8 and 10). We next examined the reason for this using X-ray structures.

Figure 7 shows bird's eye views of **1f**, **1d**, and the bis(trimethylsilyl) analogue of **1e** (**1e′**). The PPh_3 ligands which are located above and below the ruthenium are omitted for clarity. The structures of **1d** and **1e′** are taken from the literature,[23,29] while that of **1f** was confirmed in this study.[30]

Organoruthenium(II) complexes with a d^6 metal center have the propensity to make a square-pyramidal structure bearing a highly electron-donating ligand at the apical position.[31] All of the complexes in Figure 7 essentially possess such structural features. Thus, the most donating alkenyl ligand is located at the apical position, and the two PPh_3 groups and the carbonyl ligand occupy three of the four corners of the coordination square, respectively. The only exception is the orientation of the chloride ligand. Thus, as judged from the alkenyl(C^α)−Ru−Cl angles, its location significantly deviates from the ideal coordination plane, reflecting the steric demand of alkenyl ligands. The flexibility of the Ru−Cl bond may be attributed to its ionic bonding character.

It is clearly seen that the *p*-methoxystyryl complex **1f** has the space capable of accepting direct interaction with hydrosilane. It is convincing that the other styryl complexes (**1b**, **1g**−**k**) employed in this study have similar structural features as well. The approach of hydrosilane toward ruthenium should take place initially from the compact and electron-rich hydrogen atom.[16a] This process may involve enlargement of the alkenyl(C^α)−Ru−Cl angle, resulting from the flexible Ru−Cl bond (Scheme 3). The electrophilic nature of the hydrosilane is enhanced by this coordination, leading to nucleophilic attack of the α-carbon of the styryl ligand on silicon (Scheme 5). The four-center transition state thus formed gives rise to the selective formation of Ru−H and Si−C bonds (path A, mechanism I in Scheme 4).

In contrast, the space for the interaction with hydrosilane in **1d** and **1e** is effectively blocked by phenyl (**1d**) or silylethenyl (**1e**) groups at the α-position of alkenyl ligands. Consequently, these complexes must dissociate one of the PPh_3 ligands prior to the interaction with hydrosilane (Schemes 6 and 7). As supported by the kinetic data for **1e**, the coordinatively unsaturated species thus produced (**8d** and **8e**) undergo oxidative addition of hydrosilane to give hydrido(organo)silylruthenium(IV) intermediates, which reductively eliminate the C−H coupling products (**4**) along with the formation of silylruthenium (path B, mechanism IV in Scheme 8).

Conclusions

We have demonstrated that the C−Si and C−H bond formation from alkenylruthenium(II) complexes and hydrosilane exhibit clearly different kinetic behavior from each other. Although it might be hard to eliminate explicitly the possibility of the oxidative addition−reductive elimination process, all of the kinetic data observed for the C−Si bond formation from styryl complexes (**1b**, **1f**−**k**) (path A) have been reasonably accounted for by a σ-bond metathesis process, which is initiated by direct association of the styrylruthenium with hydrosilane, followed by nucleophilic attack of the styryl ligand on silicon. This mechanism resembles "the adduct formation mechanism", previously proposed for the silane alcoholysis catalyzed by a cationic iridium(III) complex,[12a] in which nucleophilic attack of a coordinated alcohol on an η^2-hydrosilane ligand was postulated to be preferred over the conventional oxida-

(27) (a) Palmer, B. J.; Hill, R. H. *Can. J. Chem.* **1996**, *74*, 1959. (b) Hostetler, M. J.; Buees, M. D.; Bergman, R. G. *Organometallics* **1993**, *12*, 65. (c) Hostetler, M. J.; Bergman, R. G. *J. Am. Chem. Soc.* **1992,** *114*, 7629. (d) Hester, D. M.; Sun, J.; Harper, A. W.; Yang, G. K. *J. Am. Chem. Soc.* **1992**, *114*, 5234. (e) Hill, R. H.; Wrighton, M. S. *Organometallics* **1985**, *4*, 413. (f) Hill, R. H.; Wrighton, M. S. *Organometallics* **1987**, *6*, 632.

(28) (a) Abis, L.; Sen, A.; Halpern, J. *J. Am. Chem. Soc.* **1978**, *100*, 2915. (b) Michelin, R. A.; Faglia, S.; Uguagliati, P. *Inorg. Chem.* **1983**, *22*, 1831. (c) Okrasinski, S. J.; Norton, J. R. *J. Am. Chem. Soc.* **1977**, *99*, 295. (d) Keyes, M. C.; Young, V. G., Jr.; Tolman, W. B. *Organometallics* **1996**, *15*, 4133. (e) Harper, T. G. P.; Desrosiers, P. J.; Flood, T. C. *Organometallics* **1990**, *9*, 2523. (f) Ittel, S. D.; Tolman, C. A.; English, A. D.; Jesson, J. P. *J. Am. Chem. Soc.* **1978**, *103*, 3396. (g) Parkin, G.; Bercaw, J. E. *Organometallics* **1989**, *8*, 1172. (h) Buchanan, J. M.; Stryker, J. M.; Bergman, R. G. *J. Am. Chem. Soc.* **1986**, *108*, 1537. (i) Jones, W. D.; Feher, F. J. *J. Am. Chem. Soc.* **1984**, *106*, 1650.

(29) (a) Torres, M. R.; Vegas, A.; Santos, A. *J. Organomet. Chem.* **1986**, *309*, 169. (b) Torres, M. R.; Vegas, A.; Santos, A.; Ros, J. *J. Organomet. Chem.* **1987**, *326*, 413.

(30) Details of the X-ray structure of **1f** are reported in the Supporting Information.

(31) Albright, T. A.; Burdett, J. K.; Whangbo, M. H. *Orbital Interactions in Chemistry*; Wiley: New York, 1985; p 310.

tive addition process. Common features for both reactions are occurrence of a nucleophilic attack on the coordinated hydrosilane and negligible k_{H-Si}/k_{D-Si} value. On the other hand, the C−H bond formation from **1d** and **1e** (path B) has been suggested to involve a Ru(IV) intermediate which is formed by dissociation of PPh_3, followed by oxidative addition of hydrosilane.

It should be noted that the C−Si and C−H bond formation selectively produce hydrido- and silylruthenium complexes, respectively, which are the key intermediates for the Chalk−Harrod and modified Chalk−Harrod cycles. The reaction courses are mainly dictated by steric conditions around the ruthenium, which control the reaction processes without or with the dissociation of PPh_3. The former leads to the C−Si bond formation, while the latter gives rise to the C−H bond formation.

Experimental Section

General Considerations. All manipulations were carried out under a nitrogen atmosphere using standard Schlenk techniques. Nitrogen gas was dried by passage through P_2O_5 (Merck, SICAPENT). NMR spectra were recorded on a Varian Mercury 300 (^{1}H NMR, 300.106 MHz; ^{13}C NMR, 75.470 MHz; ^{31}P NMR, 121.486 MHz) spectrometer. Chemical shifts are reported in δ (ppm) referred to an internal $SiMe_4$ standard for ^{1}H and ^{13}C NMR and to an external 85% H_3PO_4 standard for ^{31}P NMR. Mass spectra were measured using a Shimadzu QP-5000 GC−mass spectrometer (EI, 70 eV, capillary column). GLC analysis was performed with a GL Sciences GC-353 instrument equipped with a FID detector and a capillary column (TC-1, 30 m). THF, Et_2O, benzene, and hexane were dried over sodium benzophenone ketyl and distilled just before using. CH_2Cl_2 was dried over CaH_2 and distilled just before using. $CDCl_3$ was purified by passage though an Al_2O_3 column and dried over molecular sieves 4A. The complexes $RuHCl(CO)(PPh_3)_3$ (**2**),[32] $Ru(CH{=}CHPh)Cl(CO)(PPh_3)_2$ (**1b**),[29a] Ru[CH=CH(*t*-Bu)]Cl(CO)$(PPh_3)_2$ (**1c**),[29b] $Ru(CPh{=}CHPh)Cl(CO)(PPh_3)_2$ (**1d**),[29a] and Ru[C(=CHSiMe$_2$Ph)CH=CHSiMe$_3$]Cl(CO)$(PPh_3)_2$ (**1e**)[8] were synthesized according to the literature. All other compounds were obtained from commercial sources and used without purification.

Preparation of Para-Substituted Styryl Complexes (1f−k). The preparation of Ru[CH=CH(C_6H_4-*p*-OMe)]Cl(CO)$(PPh_3)_2$ (**1f**) represents a typical example. The complex $RuHCl(CO)(PPh_3)_3$ (**2**; 201 mg, 0.211 mmol) was dissolved in CH_2Cl_2 (10 mL) at room temperature, and (*p*-methoxyphenyl)acetylene (40 μL, 0.31 mmol) was added by means of a syringe. The yellow solution instantly turned red. After 15 min the solution was filtered through a short Florisil column and concentrated under reduced pressure. Addition of hexane (3 mL) with stirring led to precipitation of an orange solid, which was collected by filtration, washed with hexane (2 mL × 2), and dried under vacuum. The crude product was dissolved in CH_2Cl_2 (1 mL), and Et_2O (3 mL) was carefully layered. The solvent layers were mixed slowly at −20 °C to give red crystals of **1f**, which contains 1 equiv of Et_2O in the crystal (127 mg, 73% yield). ^{1}H NMR ($CDCl_3$): δ 8.13 (dt, J = 13.2 and 2.2 Hz, 1H, =CH), 7.60−7.53 (m, 12H, Ph), 7.43−7.33 (m, 18H, Ph), 6.70 (s, 4H, C_6H_4), 5.50 (dt, J = 13.2 and 2.2 Hz, 1H, =CH), 3.76 (s, 3H, OCH_3), 3.47 (q, J = 7.0 Hz, 4H, Et_2O), 1.20 (t, J = 7.0 Hz, 6H, Et_2O). ^{13}C{^{1}H} NMR ($CDCl_3$): δ 201.7 (t, J = 14 Hz, CO), 156.9 (s, C_6H_4), 143.0 (br, Ru*C*H=CH), 134.7 (s, RuCH=*C*H), 134.1 (virtual triplet, J = 6 Hz, PPh), 132.2 (s, C_6H_4), 131.8 (virtual triplet, J = 21 Hz, PPh), 130.1 (s, PPh), 128.3 (virtual triplet, J = 5 Hz, PPh), 125.4 (s, C_6H_4), 113.5 (s, C_6H_4), 65.8 (s, Et_2O), 55.2 (s, MeO), 15.3 (s, Et_2O). ^{31}P{^{1}H} NMR ($CDCl_3$): δ 31.3 (s). IR (KBr): ν_{CO} 1923 cm^{-1}. Anal. Calcd for $C_{46}H_{39}ClO_2P_2Ru{\cdot}C_4H_{10}O$: C, 66.00; H, 5.51. Found: C, 65.82; H, 5.40.

Complexes **1g**−**k** were similarly prepared and isolated as red crystals by recrystallization from CH_2Cl_2/Et_2O. The spectroscopic and analytical data are as follows.

Ru[CH=CH(C_6H_4-*p*-Me)]Cl(CO)$(PPh_3)_2$ (1g). Yield: 74%. ^{1}H NMR ($CDCl_3$): δ 8.35 (dt, J = 13.0 and 2.1 Hz, 1H, =CH), 7.59−7.53 (m, 12H, Ph), 7.52−7.33 (m, 18H, Ph), 6.96 (d, J = 8.1 Hz, 2H, C_6H_4), 6.70 (d, J = 8.1 Hz, 2H, C_6H_4), 5.55 (dt, J = 13.0 and 2.1 Hz, 1H, =CH), 2.23 (s, 3H, Me). ^{13}C{^{1}H} NMR ($CDCl_3$): δ 201.7 (t, J = 14 Hz, CO), 145.3 (t, J = 12 Hz, Ru*C*H=CH), 136.2 (s, C_6H_4), 135.1 (t, J = 4 Hz, RuCH=*C*H), 134.2 (virtual triplet, J = 6 Hz, PPh), 133.8 (s, C_6H_4), 131.8 (virtual triplet, J = 21 Hz, PPh), 130.1 (s, PPh), 128.8 (s, C_6H_4), 128.3 (virtual triplet, J = 5 Hz, PPh), 124.4 (s, C_6H_4), 21.0 (s, Me). ^{31}P{^{1}H} NMR ($CDCl_3$): δ 31.1 (s). IR (KBr): ν_{CO} 1923 cm^{-1}. Anal. Calcd for $C_{46}H_{39}ClOP_2Ru$: C, 68.53; H, 4.88. Found: C, 68.82; H, 5.02.

Ru[CH=CH(C_6H_4-*p*-F)]Cl(CO)$(PPh_3)_2$ (1h). Yield: 66%. ^{1}H NMR ($CDCl_3$): δ 8.28 (dt, J = 13.2 and 2.1 Hz, 1H, =CH), 7.58−7.52 (m, 12H, Ph), 7.44−7.34 (m, 18H, Ph), 6.81 (t, J = 8.8 Hz, 2H, C_6H_4), 6.69 (t, J = 8.8 Hz, 2H, C_6H_4). ^{13}C{^{1}H} NMR ($CDCl_3$): δ 201.6 (t, J = 16 Hz, CO), 160.4 (d, $^1J_{C-F}$ = 243 Hz, C_6H_4), 145.9 (br, Ru*C*H=CH), 135.1 (s, RuCH=*C*H), 134.2 (virtual triplet, J = 6 Hz, PPh), 131.7 (virtual triplet, J = 22 Hz, PPh), 130.2 (s, PPh), 128.3 (virtual triplet, J = 5 Hz, PPh), 125.4 (d, $^3J_{C-F}$ = 8 Hz, C_6H_4), 114.7 (d, $^2J_{C-F}$ = 21 Hz, C_6H_4). One carbon signal of the C_6H_4F ring could not be detected, probably due to overlapping. ^{31}P{^{1}H} NMR ($CDCl_3$): δ 31.4 (s). IR (KBr): ν_{CO} 1912 cm^{-1}. Anal. Calcd for $C_{45}H_{36}ClFOP_2Ru$: C, 66.71; H, 4.48. Found: C, 66.50; H, 4.47.

Ru[CH=CH(C_6H_4-*p*-Cl)]Cl(CO)$(PPh_3)_2{\cdot}Et_2O$ (1i·Et_2O). Yield: 57%. ^{1}H NMR ($CDCl_3$): δ 8.44 (dt, J = 13.5 and 2.1 Hz, 1H, =CH), 7.57−7.51 (m, 12H, Ph), 7.45−7.33 (m, 18H, Ph), 7.08 (d, J = 8.4 Hz, 2H, C_6H_4), 6.66 (d, J = 8.4 Hz, 2H, C_6H_4), 5.50 (dt, J = 13.5 and 2.1 Hz, 1H, =CH), 5.51 (dt, J = 13.0 and 2.1 Hz, 1H, =CH), 3.47 (q, J = 7.0 Hz, 4H, Et_2O), 1.20 (t, J = 7.0 Hz, 6H, Et_2O). ^{13}C{^{1}H} NMR ($CDCl_3$): δ 201.4 (t, J = 15 Hz, CO), 148.3 (t, J = 11 Hz, Ru*C*H=CH), 137.0 (t, J = 2 Hz, RuCH=*C*H), 134.1 (virtual triplet, J = 6 Hz, PPh), 131.6 (virtual triplet, J = 22 Hz, PPh), 130.2 (s, PPh, para), 129.7 (s, C_6H_4), 128.3 (virtual triplet, J = 5 Hz, PPh), 128.2 (s, C_6H_4), 125.4 (s, C_6H_4), 65.8 (s, Et_2O), 15.3 (s, Et_2O). ^{31}P-{^{1}H} NMR ($CDCl_3$): δ 31.6 (s). IR (KBr): ν_{CO} 1925 cm^{-1}. Anal. Calcd for $C_{45}H_{36}Cl_2OP_2Ru{\cdot}C_4H_{10}O$: C, 65.33; H, 5.15. Found: C, 65.08; H, 4.92.

Ru[CH=CH(C_6H_4-*p*-Br)]Cl(CO)$(PPh_3)_2{\cdot}Et_2O$ (1j·Et_2O). Yield: 69%. ^{1}H NMR ($CDCl_3$): δ 8.50 (dt, J = 13.4 and 2.0 Hz, 1H, =CH), 7.57−7.51 (m, 12H, Ph), 7.45−7.31 (m, 18H, Ph), 7.23 (d, J = 8.4 Hz, 2H, C_6H_4), 6.62 (d, J = 8.4 Hz, 2H, C_6H_4), 5.49 (dt, J = 13.4 and 2.0 Hz, 1H, =CH), 3.47 (q, J = 7.0 Hz, 4H, Et_2O), 1.20 (t, J = 7.0 Hz, 6H, Et_2O). ^{13}C{^{1}H} NMR ($CDCl_3$): δ 201.5 (t, J = 14 Hz, CO), 148.9 (t, J = 11 Hz, Ru*C*H=CH), 137.4 (s, RuCH=*C*H), 134.1 (virtual triplet, J = 6 Hz, PPh), 131.6 (virtual triplet, J = 22 Hz, PPh), 131.1 (s, C_6H_4), 130.2 (s, PPh), 128.3 (virtual triplet, J = 5 Hz, PPh), 125.8 (s, C_6H_4), 117.7 (s, C_6H_4), 65.8 (s, Et_2O), 15.3 (s, Et_2O). ^{31}P{^{1}H} NMR ($CDCl_3$): δ 31.4 (s). IR (KBr): ν_{CO} 1925 cm^{-1}. Anal. Calcd for $C_{45}H_{36}BrClOP_2Ru{\cdot}C_4H_{10}O$: C, 62.26; H, 4.91. Found: C, 61.58; H, 4.68.

Ru[CH=CH(C_6H_4-*p*-CF_3)]Cl(CO)$(PPh_3)_2{\cdot}Et_2O$ (1k·Et_2O). Yield: 66%. ^{1}H NMR ($CDCl_3$): δ 8.76 (dt, J = 13.4 and 2.0 Hz, 1H, =CH), 7.57−7.50 (m, 12H, Ph), 7.45−7.33 (m, 20H, Ph and C_6H_4), 6.81 (d, J = 8.2 Hz, 2H, C_6H_4), 5.60 (dt, J = 13.4 and 2.0 Hz, 1H, =CH), 3.47 (q, J = 7.0 Hz, 4H, Et_2O), 1.20 (t, J = 7.0 Hz, 6H, Et_2O). ^{13}C{^{1}H} NMR ($CDCl_3$): δ 201.3 (t, J = 14 Hz, CO), 152.6 (br, Ru*C*H=CH), 141.4 (s, C_6H_4), 134.3 (s, RuCH=*C*H), 134.1 (virtual triplet, J = 6 Hz, PPh),

(32) Ahmad, N.; Levison, J. J.; Robinson, S. D.; Uttley, M. F. *Inorg. Synth.* **1974**, *15*, 45.

131.5 (virtual triplet, J = 22 Hz, PPh), 130.3 (s, PPh), 128.4 (virtual triplet, J = 5 Hz, PPh), 125.8 (q, $^2J_{C-F}$ = 32 Hz, C_6H_4), 125.1 (q, $^3J_{C-F}$ = 4 Hz, C_6H_4), 124.6 (q, $^1J_{C-F}$ = 272 Hz, CF_3), 124.1 (s, C_6H_4), 65.8 (s, Et_2O), 15.3 (s, Et_2O). $^{31}P\{^1H\}$ NMR ($CDCl_3$): δ 31.6 (s). IR (KBr): ν_{CO} 1926 cm^{-1}. Anal. Calcd for $C_{46}H_{36}F_3ClOP_2Ru\cdot C_4H_{10}O$: C, 64.27; H, 4.96. Found: C, 64.51; H, 4.94.

Reactions of Alkenyl Complexes with $HSiMe_2Ph$ (Table 1). A typical procedure (run 2) is as follows. Complex **1b** (4.8 mg, 6.0 μmol) and PPh_3 (1.6 mg, 6.0 mmol) were loaded in an NMR sample tube equipped with a rubber septum cap, and the system was replaced with nitrogen gas. Anisole (1.0 μL, 9.2 μmol) was added as an internal standard for ^1H NMR analysis. All contents were dissolved in $CDCl_3$ (0.6 mL) at room temperature and then cooled to −40 °C. $HSiMe_2Ph$ (16.4 mg, 0.120 mmol) was added, and the sample solution was warmed to 30 °C. The color of the solution instantly changed from red to orange. $^{31}P\{^1H\}$ NMR analysis revealed the absence of **1b** and the formation of the hydride complex **2** in over 99% selectivity. The amounts of *trans*-PhCH=CHSiMe$_2$Ph (**4b**)[33] and styrene (**5b**) produced were determined on the basis of the relative peak integration of olefinic protons of **4b** (δ 6.78 (d)) and **5b** (δ 5.73 (d)) to anisole (δ 3.81 (s)) in the ^1H NMR spectrum. The formation of **4b** and **5b** was confirmed also by GC-MS spectrometry.

The reactions of **1c**−**e** with $HSiMe_2Ph$ were similarly examined. The ratio of $RuHCl(CO)(PPh_3)_3$ (**2**; δ 39.6 (br) and 13.5 (br)) to $Ru(SiMe_2Ph)Cl(CO)(PPh_3)_2$ (**3**;[8,34] δ 33.4 (s)) was determined by $^{31}P\{^1H\}$ NMR spectroscopy. Organic products were analyzed by ^1H NMR spectroscopy and GC-MS spectrometry. All are known compounds: *t*-BuCH=CHSiMe$_2$Ph (**4c**),[33] (1*E*,3*E*)-1-(dimethylphenylsilyl)-4-(trimethylsilyl)-1,3-butadiene (**5e′**),[8] and 1-(dimethylphenylsilyl)-4-(trimethylsilyl)-2-butene (**5e″**).[8]

Kinetic Study on the Reaction of 1b with $HSiMe_2Ph$ (Table 2). A typical procedure (run 4) is as follows. Complex **1b** (4.8 mg, 6.0 μmol) and PPh_3 (1.6 mg, 6.0 μmol) were loaded in an NMR sample tube equipped with a rubber septum cap, and the system was replaced with nitrogen gas. Anisole (1 μL, 9.2 μmol) was added. All contents were dissolved in $CDCl_3$ (ca. 0.5 mL) at room temperature. $HSiMe_2Ph$ (16.4 mg, 0.120 mmol) was added at −40 °C, and the volume of the solution was adjusted with additional $CDCl_3$ exactly to 0.60 mL. The sample was placed in an NMR sample probe controlled to 10.0 ± 0.1 °C. The amounts of **1b** at intervals were determined by measuring the relative peak integration of the olefinic proton signal of **1b** at δ 5.58 and the methyl proton signal of anisole at δ 3.81 in ^1H NMR spectra.

Kinetic runs with the series of para-substituted styryl complexes **1f**−**k** were similarly conducted. The product styrylsilanes were identified by ^1H NMR spectroscopy and GLC analysis using authentic samples, which were prepared by catalytic hydrosilylation of phenylacetylene derivatives.

Catalytic Hydrosilylation of Para-Substituted Phenylacetylenes with $HSiMe_2Ph$. A typical procedure is as follows. To a Schlenk tube containing a catalytic amount of $RuHCl(CO)(PPh_3)_3$ (50.0 mg, 0.0525 mmol) were added CH_2Cl_2 (1 mL), (*p*-methoxyphenyl)acetylene (137 mg, 1.05 mmol), and $HSiMe_2Ph$ (157 mg, 1.15 mmol) at room temperature. The mixture was stirred at 30 °C for 3 h. GLC analysis revealed the absence of the starting acetylene and the selective formation of *trans*-(*p*-$MeOC_6H_4$)CH=CHSiMe$_2$Ph (**4f**), which was isolated by column chromatography (SiO_2, CH_2Cl_2) followed by bulb-to-bulb distillation under reduced pressure (258 mg, 92% yield). ^1H NMR ($CDCl_3$): δ 7.59−7.52 (m, 3H, Ar), 7.41−7.32 (m, 6H, Ar), 6.88 (d, J = 18.9 Hz, 1H, =CHAr), 6.41 (d, J = 18.9 Hz, 1H, =CHSi), 3.81 (s, 3H, MeO), 0.42 (s, 6H, $SiMe_2$). MS (*m*/*z* (relative intensity, %)): 268 (M^+, 40), 253 (53), 176 (17), 175 (100), 145 (39), 121 (33), 105 (17), 59 (21), 43 (56). Identification data for the other hydrosilylation products are as follows.

***trans*-(*p*-MeC_6H_4)CH=CHSiMe$_2$Ph (4g).** ^1H NMR ($CDCl_3$): δ 7.62−7.33 (m, 7H, Ar), 7.13 (d, J = 8.1 Hz, 2H, Ar), 6.91 (d, J = 18.9 Hz, 1H, =CHAr), 6.51 (d, J = 18.9 Hz, 1H, =CHSi), 2.34 (s, 3H, Me), 0.41 (s, 6H, $SiMe_2$). MS (*m*/*z* (relative intensity, %)): 252 (M^+, 37), 237 (58), 160 (29), 159 (100), 145 (41), 135 (17), 121 (35), 118 (17), 105 (19), 43 (56).

***trans*-(*p*-FC_6H_4)CH=CHSiMe$_2$Ph (4h).** ^1H NMR ($CDCl_3$): δ 7.67−7.31 (m, 7H, Ar), 7.02 (t, J = 8.7 Hz, 2H, Ar), 6.90 (d, J = 18.9 Hz, 1H, =CHAr), 6.50 (d, J = 18.9 Hz, 1H, =CHSi), 0.44 (s, 6H, $SiMe_2$). MS (*m*/*z* (relative intensity, %)): 256 (M^+, 27), 241 (54), 164 (15), 163 (100), 145 (27), 121 (52), 105 (18), 53 (15), 47 (30), 43 (64).

***trans*-(*p*-ClC_6H_4)CH=CHSiMe$_2$Ph (4i).** ^1H NMR ($CDCl_3$): δ 7.64−7.53 (m, 3H, Ar), 7.46−7.35 (m, 6H, Ar), 6.87 (d, J = 18.9 Hz, 1H, =CHAr), 6.56 (d, J = 18.9 Hz, 1H, = CHSi), 0.42 (s, 6H, $SiMe_2$). MS (*m*/*z* (relative intensity, %)): 274 (M + 2, 9), 272 (M^+, 26), 257 (46), 181 (28), 179 (100), 145 (28), 121 (52), 105 (21), 63 (21), 43 (74).

***trans*-(*p*-BrC_6H_4)CH=CHSiMe$_2$Ph (4j).** ^1H NMR ($CDCl_3$): δ 7.62−7.29 (m, 9H, Ar), 6.85 (d, J = 18.9 Hz, 1H, =CHAr), 6.57 (d, J = 18.9 Hz, 1H, =CHSi), 0.43 (s, 6H, $SiMe_2$). MS (*m*/*z* (relative intensity, %)): 318 (M + 2, 1), 316 (M^+, 1), 225 (3), 223 (3), 179 (4), 121 (4), 44 (100), 43 (9), 41 (3), 40 (34).

***trans*-(*p*-$CF_3C_6H_4$)CH=CHSiMe$_2$Ph (4k).** ^1H NMR ($CDCl_3$): δ 7.62−7.28 (m, 9H, Ar), 6.95 (d, J = 19.2 Hz, 1H, =CHAr), 6.70 (d, J = 19.2 Hz, 1H, =CHSi), 0.45 (s, 6H, $SiMe_2$). MS (*m*/*z* (relative intensity, %)): 306 (M^+, 34), 291 (52), 229 (34), 213 (90), 151 (72), 145 (29), 121 (88), 105 (29), 77 (27), 43 (100).

Kinetic Studies on the Reaction of 1d and 1e with $HSiMe_2Ph$. A typical procedure is as follows. Complex **1d** (5.3 mg, 6.0 μmol) and PPh_3 (1.6 mg, 6.0 μmol) were loaded in an NMR sample tube, and the system was replaced with nitrogen gas. Anisole (0.6 μL, 5.5 μL) and $HSiMe_2Ph$ (16.4 mg, 0.120 mmol) were added at 0 °C by means of syringe. The contents were dissolved in $CDCl_3$ (ca. 0.5 mL), and the volume of the solution was adjusted to 0.60 mL with additional $CDCl_3$ at room temperature. The sample tube was placed in an NMR sample probe controlled to 45.0 ± 0.1 °C, and the time course of the reaction was followed by ^1H NMR spectroscopy. The amounts of **1d** at intervals were determined on the basis of the relative peak integration of the olefinic proton signal of **1d** at δ 5.43 and the methyl proton signal of anisole at δ 3.81. Kinetic experiments on the reaction of **1e** were similarly conducted. The time course was followed by measuring the olefinic proton signal of **1e** at δ 5.84.

Acknowledgment. This work was supported by a Grant-in-Aid for Scientific Research on Priority Area "The Chemistry of Inter-element Linkage" (No. 09239105) from the Ministry of Education, Science, Sports and Culture of Japan.

Supporting Information Available: Details of the X-ray structural determination of **1f**·Et_2O, including an experimental description, an ORTEP drawing, an atomic numbering scheme, and tables of crystal data, atomic coordinates, thermal parameters, and all bond distances and angles, and tables giving kinetic data for **1d** and **1e**. This material is available free of charge via the Internet at http://pubs.acs.org.

OM9909035

(33) Jun, C.-H.; Crabtree, R. H. *J. Organomet. Chem.* **1993**, *447*, 177.

(34) Marciniec, B.; Pietraszuk, C. *Organometallics* **1997**, *16*, 4320.